

3D FEM-BEM-Coupling Method to solve Magnetostatic Maxwell Equations

Florian Bruckner^{a,*}, Christoph Vogler^a, Michael Feischl^b, Dirk Praetorius^b, Bernhard Bergmair^a, Thomas Huber^a, Markus Fuger^a, Dieter Suess^a

^aVienna University of Technology, Inst. Solid State Physics, Austria

^bVienna University of Technology, Inst. Analysis and Scientific Computing, Austria

Abstract

3D magnetostatic Maxwell equations are solved using the direct Johnson-Nédélec FEM-BEM coupling method and a reduced scalar potential approach. The occurring BEM matrices are calculated analytically and approximated by H-matrices using the ACA+ algorithm. In addition a proper preconditioning method is suggested that allows to solve large scale problems using iterative solvers.

Keywords: FEM-BEM coupling, Johnson-Nédélec method, ACA+, preconditioner, magnetostatic Maxwell equations, scalar potential

1. Introduction

For the design of various applications ranging from electric motors to write heads in hard disks the solution of 3D magnetostatic Maxwell equations is required. A straight forward method concerning implementation is the Magnetic Moment Method (MMM) [1]. It does not require a mesh in free space and can easily treat a nonlinear material law. A drawback of the method is that it leads to fully populated matrices of the size $3M \times 3M$, where M is the number of volume elements. Recently, compression techniques such as H-matrices were applied in order to reduce complexity [2]. A well established tool for the solution of partial differential equations is the Finite Element Method (FEM) which can be applied to the magnetostatic problem in its differential form. Various methods were proposed to solve this open boundary problem, such as infinite elements [3], ballooning elements [4], parallelepipedic shell transformation [5], and asymptotic boundary conditions [6]. Drawbacks of these methods are either a certain number of elements in the outer region or intrinsic systematic errors. For linear problems the Boundary Element Method (BEM) allows to transform the volume integrals arising from the open boundary problem into corresponding surface integrals, which reduces the computational complexity of the problem. In order to be able to take nonlinear material laws into account, the BEM can be merged with the FEM combining the advantages of both methods. The FEM efficiently takes into account the non-linearity of the problem, and the BEM transforms the boundary condition from infinity to the

surface of the magnet. Thus no finite elements are required outside of the magnet in order to solve the system accurately. For the strayfield calculation of a given magnetization Fredkin-Koehler proposed an elegant way, where FEM and BEM equations are calculated sequentially [7]. For the solution of the complete magnetostatic Maxwell problem direct FEM-BEM coupling schemes, as the Johnson-Nédélec coupling presented in this paper, provide robust algorithms. In this paper we combine a direct FEM-BEM coupling scheme with a H-matrix compression technique for the solution of the magnetostatic Maxwell problem. Furthermore, we present a proper preconditioner which leads to a fast and reliable solver.

The structure of the paper is as follows. Section 2 summarizes the open boundary problem and its formulation with a reduced scalar potential. The coupling of FEM and BEM is discussed in section 3 followed by the construction of the BEM matrix in section 4, where the H-matrix method is used in order to compress the involved boundary matrices. For the arising system of equations a proper preconditioner for iterative solvers is proposed in section 5. Finally section 6 shows numerical results and benchmarks for different mesh sizes.

2. Reduced Scalar Potential Formulation

We start from magnetostatic Maxwell's equations which are defined in the entire space. The full space is then divided into two partitions, since we use different representations in these regions. The region Ω^+ contains all the magnetic parts of the problem which are described by FEM, whereas Ω^- contains the surrounding non-magnetic volume described by BEM. The superscripts + and - are therefore used for physical quantities within Ω^+ or Ω^- , respectively (see Fig.

*Corresponding author

Email address: florian.bruckner@tuwien.ac.at (Florian Bruckner)

1). Maxwell's equations, the material laws in both regions, and the jump conditions at the boundary of the magnetic parts are given by

$$\operatorname{rot} \mathbf{H} = \mathbf{j} \quad \mathbf{B}^+ = \mu^+ \mathbf{H}^+ \quad (1)$$

$$\operatorname{div} \mathbf{B} = 0 \quad \mathbf{B}^- = \mu^- \mathbf{H}^- \quad (2)$$

$$\mathbf{n} \times (\mathbf{H}^+ - \mathbf{H}^-) = 0 \quad (3)$$

$$\mathbf{n} \cdot (\mathbf{B}^+ - \mathbf{B}^-) = 0 \quad (4)$$

where the current density \mathbf{j} is the source of the magnetic field strength \mathbf{H} which is related to the magnetic flux \mathbf{B} via the permeability μ . The normal vector at the boundary \mathbf{n} allows to distinguish jump conditions for the normal as well as for the parallel component of the magnetic field.

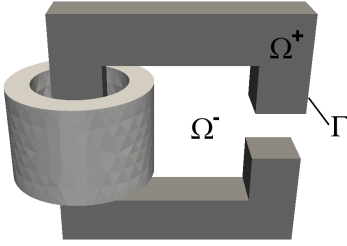


Figure 1: Example geometry for a yoke containing a magnetic region Ω^+ and the surrounding area Ω^- . In this example the external field is created by a coil located in Ω^- .

In order to reduce the number of degrees of freedom one introduces a scalar potential by splitting the total magnetic field into an external part \mathbf{H}_{ext} (which is created by currents outside of Ω^+) and the curl-free induced magnetic field which can be expressed as the gradient of a scalar potential u . Inserting this definition of the magnetic field into the Eqn. (1) - (4) leads to the following system of equations for the scalar potential u . We introduce the normal derivative of the potential at the surface of the magnetic parts as $\phi = \frac{\partial u}{\partial \mathbf{n}}$:

$$\mathbf{H} = \mathbf{H}_{\text{ext}} - \nabla u \quad (5)$$

$$\nabla \cdot (\mu^+ \nabla u^+) = \nabla \cdot (\mu^+ \mathbf{H}_{\text{ext}}) \quad (6)$$

$$\nabla^2 u^- = 0 \quad (7)$$

$$u^+ - u^- = 0 \quad (8)$$

$$\mu^+ \phi^+ - \mu^- \phi^- = (\mu^+ - \mu^-) \mathbf{n} \cdot \mathbf{H}_{\text{ext}} \quad (9)$$

If there are no currents within Ω^+ , an alternative formulation of the scalar potential can be used. In this case, the internal field H^+ is curl-free and can therefore be directly expressed as the gradient of a total scalar potential, which leads to some slightly modified

equations [8]. Since the total magnetic field can be calculated directly, numerical errors due to the subtraction of the external field are avoided. The drawback of this method is that due to the different descriptions in Ω^+ and Ω^- the potential is discontinuous at the surface of the magnet and additional complications occur if the region Ω^+ is not simply connected.

3. FEM-BEM coupling

For sake of simplicity, we restrict ourselves to linear systems. Since μ is constant the divergence operator on the right-hand side of Eqn. (6) only acts on \mathbf{H}_{ext} which gives 0.

Starting with the FEM equations for the internal problem, we use a Galerkin approach with polynomial test and shape function $\Lambda_i(\mathbf{x})$ for each node i of the problem. Transforming Eqn. (6) into the weak formulations, performing an integration by parts, and considering that for linear systems the source term on the right-hand side vanishes, leads to the following system of equations:

$$\int_{\Omega} \mu^+ \nabla \Lambda_i \cdot \nabla u^+ d\Omega - \int_{\Gamma} \mu^+ \Lambda_i \nabla u^+ \cdot \mathbf{n} d\Gamma = 0 \quad (10)$$

Using a FEM-only approach would require to define either Dirichlet or Neumann boundary conditions in order to get a solvable system. Since we do not know these boundary conditions, we introduce the normal derivatives of the potential at the boundary as new independent variables ϕ and add additional BEM equations to the system, which then has a unique solution.

For these additional equations, one recognizes that the outer potential u^- fulfills the Laplace equation. With the help of the fundamental solution $G = \frac{1}{4\pi} \frac{1}{|\mathbf{x}-\mathbf{y}|}$, u^- can be expressed by the third Green's identity in terms of its Cauchy data (the potential and its normal derivative) on the boundary Γ :

$$\frac{1}{2} u^- = \int_{\Gamma} (u^- \nabla G - \nabla u^- G) \mathbf{n} d\Gamma \quad (11)$$

Mathematically, the coupling method resulting from this approach, was first analyzed by Johnson and Nédélec [9, 10] (the $\frac{1}{2}$ factor is only valid for smooth surfaces and has to be modified at edges [11]). The terms on the right-hand side are called double-layer and single-layer potential. For a general Galerkin-BEM, formula (11) is multiplied by a test function $\Psi_m(\mathbf{x})$ and integrated over the boundary. In our implementation, we use delta distribution as test functions for the BEM equations $\Psi_m(\mathbf{x}) = \delta(\mathbf{x} - \mathbf{x}_m)$, which leads to a point-matching approach that only evaluates the equations at the centers of each boundary triangle. The main advantage of this approach is that the computation of the occurring boundary integrals is easier and less time-consuming.

Finally, we discretize our formulas by using linear shape functions Λ_j for the potential u and piecewise-constant shape functions $\mathbb{1}_n$ for its normal derivative ϕ . Furthermore, u^- and ϕ^+ can be eliminated by use of the jump conditions (8) and (9). Our discretized variables as well as the test function used within the Galerkin formalism look like the following:

$$u^+(\mathbf{x}) = \sum_j u_j \Lambda_j(\mathbf{x}) \quad \phi^-(\mathbf{x}) = \sum_n \phi_n \mathbb{1}_n(\mathbf{x}) \quad (12)$$

Combining FEM and BEM equations to one total system of equations we end up with a quadratic system M which fully defines our problem:

$$\begin{pmatrix} M_{ij}^{11} & M_{in}^{12} \\ M_{mj}^{21} & M_{mn}^{22} \end{pmatrix} \begin{pmatrix} u_j \\ \phi_n \end{pmatrix} = \begin{pmatrix} RHS_i^1 \\ \mathbf{0} \end{pmatrix} \quad (13)$$

The individual elements of the matrices can be calculated as follows. Remember that for the FEM part these matrices are sparse whereas the BEM formalism leads to dense matrices:

$$M_{ij}^{11} = \int_{\Omega} \mu^+ \nabla \Lambda_i \cdot \nabla \Lambda_j d\Omega \quad (14)$$

$$M_{in}^{12} = - \int_{\Gamma} \mu^+ \Lambda_i \mathbb{1}_n d\Gamma \quad (15)$$

$$M_{mj}^{21} = \frac{1}{2} \Lambda_j(\mathbf{x}_m) - \frac{1}{4\pi} \int_{\Gamma} \Lambda_j(\mathbf{y}) \frac{\mathbf{x}_m - \mathbf{y}}{|\mathbf{x}_m - \mathbf{y}|^3} \mathbf{n} d\Gamma_y \quad (16)$$

$$M_{mn}^{22} = \frac{1}{4\pi} \int_{\Gamma} \frac{\mathbb{1}_n(\mathbf{y})}{|\mathbf{x}_m - \mathbf{y}|} d\Gamma_y \quad (17)$$

$$RHS_i^1 = \int_{\Gamma} (\mu^+ - \mu^-) \mathbf{n} \cdot \mathbf{H}^{\text{ext}} \Lambda_i d\Gamma \quad (18)$$

The indices i, j run from 1 to the number of nodes of the geometry, whereas n, m run from 1 to the number of boundary elements. Since only boundary nodes contribute to the boundary integrals in M^{12} and M^{21} all matrix elements which correspond to nodes within the volume are equal to 0.

4. Calculation of BEM matrices

The occurring BEM matrices are calculated analytically as given in Ref. [12]. (An alternative but more special solution was given by Lindholm [11]). The single and double-layer potential (E and D) at the point \mathbf{x} created by a triangle Δ using the Greens' function of the 3 dimensional Laplacian are given by

$$E(\mathbf{x}) = \frac{1}{4\pi} \int_{\Delta} \frac{f(\mathbf{y})}{|\mathbf{x} - \mathbf{y}|} d\Gamma_y \quad (19)$$

$$D(\mathbf{x}) = \frac{1}{4\pi} \int_{\Delta} f(\mathbf{y}) \frac{\mathbf{x} - \mathbf{y}}{|\mathbf{x} - \mathbf{y}|^3} \mathbf{n} d\Gamma_y \quad (20)$$

where $f(\mathbf{y})$ stands for the shape function of the used elements. For our implementation we confine ourselves to piecewise constant shape function for the single-layer potential and linear shape functions for the double-layer potential. Since these integrals are translation- and rotation-invariant, we use a transformation Φ to rotate the triangle into the x_1 - x_2 -plane and to move the reference point \mathbf{x} onto the x_3 axis (see Fig. 2). Doing this, we can write a general polynomial shape function as $f(\mathbf{y}) = \sum_{jk} f_{jk} y_1^j y_2^k$ and we can break the problem down to the calculation of the integrals for the individual monomials that occur within the sum:

$$E_{jk}(\mathbf{x}) = \frac{1}{4\pi} \int_{\Delta} \frac{y_1^j y_2^k}{\sqrt{y_1^2 + y_2^2 + x_3^2}} dy_1 dy_2 \quad (21)$$

$$D_{jk}(\mathbf{x}) = \frac{x_3}{4\pi} \int_{\Delta} \frac{y_1^j y_2^k}{\sqrt{y_1^2 + y_2^2 + x_3^2}^3} dy_1 dy_2 \quad (22)$$

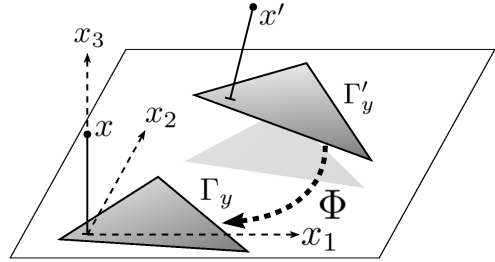


Figure 2: Diagram schematizing the triangle area used for the integration process.

The divergence theorem $\int_{\Delta} \text{div } \mathbf{G} d\Gamma = \int_{\gamma} \mathbf{G} \mathbf{n} d\gamma$ can be used to further simplify the calculation by transforming the surface integrals to line integrals [13]. One can finally derive a recursive formula for the higher order surface integrals that only depends on lowest order line integrals which can be solved analytically as well as on the lowest order double-layer term D_{00} . Furthermore D_{00} can be expressed as the surface angle corresponding to \mathbf{x} and Δ which allows a simple geometric interpretation of these terms. For the construction of the surface angle one connects \mathbf{x} with the three corners of the triangle. The intersection points of these connection lines with the unit sphere define the corners of a spherical triangle on the unit sphere. The area of this triangle finally gives us the value of D_{00} (see Fig. 3).

Using the recursive formula [13] allows to calculate the occurring integrals for shape functions of any order. For sake of clarity we now demonstrate how this recursion is derived for the lowest order single-layer potential that is used in our algorithm. If we set $\mathbf{G} = \left(\frac{y_1}{r}, \frac{y_2}{r}\right)$ with $\text{div } \mathbf{G} = \frac{1}{r} + \frac{x_3^2}{r^3}$ and $r = \sqrt{y_1^2 + y_2^2 + x_3^2}$

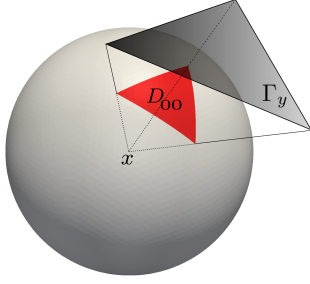


Figure 3: D_{00} can be interpreted as the surface of the triangle on the unit sphere.

the divergence theorem gives:

$$\underbrace{\int \frac{1}{r}}_{4\pi E_{00}} + x_3^2 \underbrace{\int \frac{1}{r^3}}_{4\pi x_3 D_{00}} = \int_{\gamma} \left(\frac{y_1}{r}, \frac{y_2}{r} \right) \mathbf{n} d\gamma \quad (23)$$

We can now calculate the interaction matrix elements of the piecewise constant single-layer shape functions E_{00} , by means of the line integral on the right-hand side of equation (23) as well as of the surface angle D_{00} .

The main numerical problem when dealing with BEM matrices is that they are dense, and thus extensive computation time and storage capacity is needed to handle them. This problem can be overcome by use of H-matrices [14], where some blocks of the dense matrices (\mathbf{M}^{21} , \mathbf{M}^{22}) are replaced by low rank approximations. If a block can be simplified or not depends on the admissibility criterion which tells whether the size of the corresponding pointsets is smaller than the distance between source and destination pointset. If the admissibility criterion is fulfilled, the corresponding block describes far-field interaction and thus can be approximated without introducing a significant error. On the other hand if source and destination pointsets are very close to each other, then the corresponding matrix is stored as a full matrix in order to obtain a sufficient accuracy.

We use the ACA+ algorithm which allows to obtain low-rank approximations without having to evaluate all elements of the original block [15]. Therefore the approximated system matrix of rank k is expressed as $\tilde{\mathbf{M}}^{n \times m} = \mathbf{U}^{n \times k} \mathbf{V}^{k \times m}$. \mathbf{U} and \mathbf{V} are created by sequentially extracting lines and columns of the original matrix $\mathbf{M}^{m \times n}$. Lines and columns of the matrix are chosen in a way that the biggest elements of the error matrix $\mathbf{R} = \mathbf{M} - \tilde{\mathbf{M}}$ are eliminated.

5. Preconditioning

In order to solve the system of equations, we use an iterative solver (KINSOL [16]) which is an efficient method for large non-linear systems. It performs an Inexact Newton iteration for general non-linear problems. Each step of the non-linear iteration requires the

solution of a linear system of equations. For this purpose KINSOL uses the Generalized Minimal RESidual (GMRES) Krylov subspace method.

For linear system one can define a condition number of the system matrix \mathbf{M} which is directly related to the convergence speed of the iterative method and can be expressed as $\text{cond}(\mathbf{M}) = \|\mathbf{M}\| \|\mathbf{M}^{-1}\|$ (with a proper matrix norm). We empirically found that the condition number is directly proportional to the susceptibility of the simulated material for various models (see Fig. 6). Therefore, especially for systems with high permeability, computation time can be decreased significantly by use of a proper preconditioner.

In our current implementation, we use the preconditioning feature of the solver suite, that does a right-preconditioning, where one rewrites the original matrix equation as $(\mathbf{M}\mathbf{P}^{-1})(\mathbf{P}\mathbf{x}) = \mathbf{RHS}$, with a preconditioner matrix \mathbf{P} and the unknowns $\mathbf{x} = (u_j, \phi_n)$. This leads to a new system matrix $\mathbf{M}\mathbf{P}^{-1}$ for the iterative solver with a smaller condition number.

The preconditioner matrix \mathbf{P} is a good approximation of the system matrix \mathbf{M} , but it is easier to solve. The most time consuming part of solving the system of equations is due to the dense boundary matrices. For BEM matrices it can be proven that simple diagonal scaling reasonably improves conditioning [17].

For the coupled system numerical studies showed that using only the diagonal elements of the single-layer matrix as well as only the elements contributing to the $\frac{1}{2}$ factor within the double-layer matrix leads to a sparse approximation of the system matrix \mathbf{M} which can be used as an efficient preconditioner:

$$\mathbf{P} = \begin{pmatrix} M_{ij}^{11} & M_{in}^{12} \\ \frac{1}{2}\Lambda_j(\mathbf{x}_m) & \text{diag}(M_{mn}^{22}) \end{pmatrix} \quad (24)$$

For all our test geometries, computation times could be decreased dramatically, and additionally it does no longer depend on the used susceptibility. Results are presented in the following section.

6. Results

In this section, the algorithm is applied to calculate the induced magnetization of a magnetic sphere with susceptibility χ exposed to a homogeneous external field and a yoke magnetized by an electric coil. Since the solution for the magnetic sphere in an external field can be calculated analytically, it is well suited to check the accuracy of our algorithm. The second example shows a more advanced application of our algorithm.

6.1. Sphere

The analytical calculation of the homogeneously magnetized sphere (with a magnetization M) shows that the induced field H_d is also homogeneous within the sphere and its value is $-\frac{1}{3}M$. Adding the material law $M = \chi H$, where H is the total field $H =$

$H_d + H_{ext}$ and χ is the magnetic susceptibility of the material, directly leads to the analytical result:

$$M = \frac{3\chi}{3 + \chi} H_{ext} \quad (25)$$

The comparison of the numerical results with Eqn. (25) shows that the mean magnetization (averaged over the volume of the sphere) differs by around 0.1% using 10535 elements. In order to demonstrate the performance of the presented algorithm we measured runtime and maximal memory consumption for different number of elements (see Table 1). For high susceptibilities the problem becomes more difficult to solve due to the large condition number. For practical applications the largest relevant susceptibility is around $\chi = 10^5$, which we therefor use for our studies. The calculated magnetization for a sphere with 1074 elements is shown in Fig. 4.

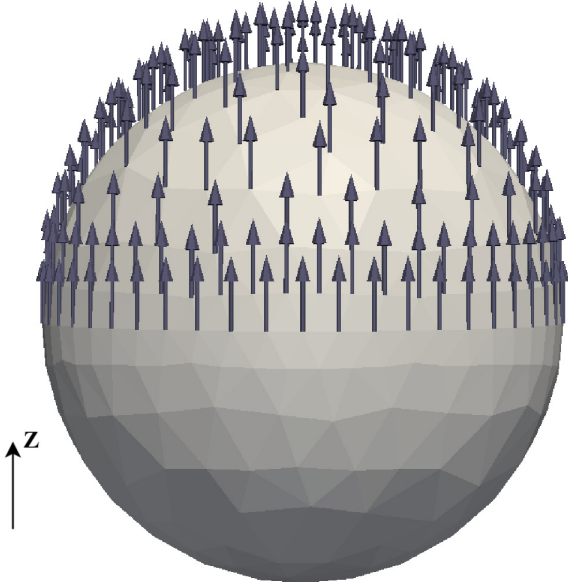


Figure 4: Simulation results for the magnetization of the magnetic sphere in a homogeneous external field. The Magnetization is nearly perfectly aligned to the external field which is applied in z direction.

| No. elements | 1074 | 10535 | 337505 | 1546384 |
|--------------|-------|-------|--------|---------|
| runtime [s] | 1.470 | 26.45 | 1590.3 | 25324.1 |
| memory [MB] | 194 | 248 | 1499 | 5503 |

Table 1: Performance values of the sphere example for different grid sizes.

6.2. Coil and yoke

This more complex example shows a cylindrical coil around a magnetic yoke. The external field H_{ext} is created by a coil and is directly calculated by the Biot-Savart law. We again measured solver runtime as

| No. elements | 1077 | 10205 | 109384 | 1180305 |
|--------------|-------|-------|--------|---------|
| runtime [s] | 5.027 | 28.33 | 734.3 | 14035.4 |
| memory [MB] | 218 | 374 | 1025 | 5782 |

Table 2: Performance values of the yoke example for different grid sizes.

well as maximum memory consumption for different discretizations (see Table 2). The calculated magnetization for $\chi = 10^6$ can be seen in Fig. 5.

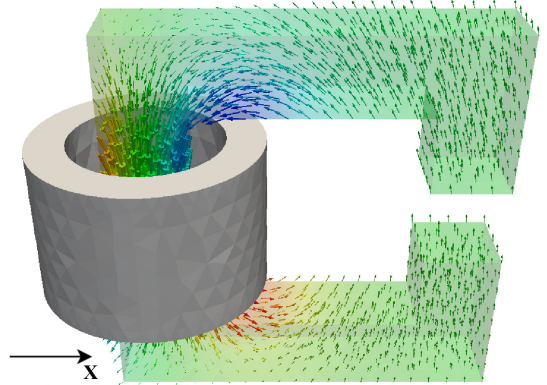


Figure 5: Simulation results for a magnetic yoke magnetized by an electric coil. 10205 elements were used for the discretization of the yoke. The color of the arrows shows the x component of the magnetization.

The calculated condition numbers as well as the computation time of the equation solver with and without preconditioning is illustrated for the yoke example in Fig. 6.

7. Conclusion

We have introduced a FEM / BEM coupling method which combines the advantages of both methods. The algorithm is applied to a magnetostatic problem with open boundary. The arising dense boundary matrices are approximated by H-matrices in order to speed up computation and to decrease memory consumption. Furthermore an effective preconditioner has been proposed in order to improve the convergence of the iterative solver. Finally the performance of the algorithm is demonstrated by two different example calculations.

Acknowledgment

The authors would like to thank the WWTF Project MA09-029 and FWF Project SFB-ViCoM F4112-N13 for the financial support.

- [1] Y. Takahashi, S. Wakao, A. Kameari, Large-Scale and highly accurate magnetic field analysis of magnetic shield, J. Appl. Phys. 99.

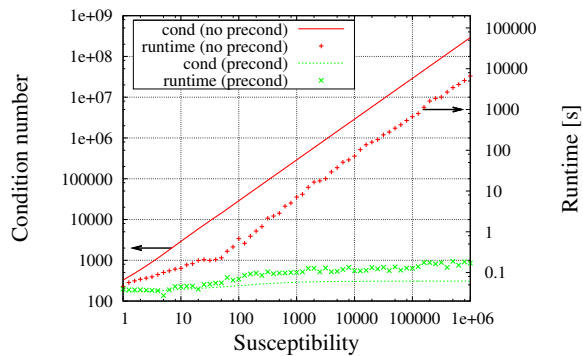


Figure 6: Condition number and solver runtime of the Yoke example (description see section 6.2) with and without preconditioner. The condition number gives a good estimation of the solver runtime. One can see that the performance is improved significantly, especially for high susceptibilities. This behavior could also be confirmed for different models, which allows to conclude that the described method should also work for arbitrary models.

- [2] Y. Takahashi, C. Matsumoto, S. Wakao, Large-Scale and fast nonlinear magnetostatic field analysis by the magnetic moment method with the adaptive cross approximation, *IEEE Trans. Magn.* 43 (2007) 1277–1280.
- [3] P. Bettess, Infinite elements, *Int. J. Numer. Methods Eng.* 11 (1977) 53–64.
- [4] P. Silvester, D. Lowther, C. Carpenter, E. Wyatt, Exterior finite elements for 2-Dimensional field problems with open boundaries, *Proc. IEE* 124 (1977) 1267–1270.
- [5] X. Brunotte, G. Meunier, J. Imhoff, Finite element modeling of unbounded problems using transformations: A rigorous, powerful and easy solution, *IEEE Trans. Magn.* 28 (1992) 1663–1666.
- [6] A. Khebir, A. Kouki, R. Mittra, Asymptotic boundary conditions for finite element analysis of Three-Dimensional transmission line discontinuities, *IEEE Trans. Microwave Theory Tech.* 38 (1990) 1427–1432.
- [7] D. Fredkin, T. Koehler, Hybrid method for computing demagnetizing fields, *IEEE Trans. Magn.* 26 (1990) 415–417.
- [8] I. Mayergoyz, M. Chari, J. D’Angelo, New scalar potential formulation for Three-Dimensional magnetostatic problems, *IEEE Trans. Magn.* MAG-23 (1987) 3889–3894.
- [9] C. Johnson, J. C. Nédélec, On the coupling of boundary integral and finite element methods, *Math. Comp.* 35 (1980) 1063–1079.
- [10] F. Sayas, The validity of Johnson-Nédélec’s BEM-FEM coupling on polygonal interfaces, *SIAM J. Numer. Anal.* 47 (2009) 3451–3463.
- [11] D. Lindholm, Three-Dimensional magnetostatic fields from Point-Matched integral equations with linearly varying scalar sources, *IEEE Trans. Magn.* MAG-20 (1984) 2025–2032.
- [12] W. Hackbusch, *Integral equations: theory and numerical treatment*, Birkhäuser, 1995.
- [13] M. Rech, *Effiziente Nahfeldkubatur in der Galerkin-Randelementmethode* (2002).
- [14] W. Hackbusch, *Hierarchische Matrizen: Algorithmen und Analysis*, Springer, 2009.
- [15] L. Grasedyck, Adaptive recompression of H-matrices for BEM, *Computing* 74 (2005) 205–223.
- [16] A. Hindmarsh, P. Brown, K. Grant, S. Lee, R. Serban, D. Shumaker, C. Woodward, SUNDIALS: suite of nonlinear and differential/algebraic equation solvers, *ACM Trans. Math. Softw.* 31 (2005) 363–396.
- [17] I. Graham, W. McLean, Anisotropic mesh refinement: The conditioning of galerkin boundary element matrices and simple preconditioners, *SIAM J. Numer. Anal.* 44 (2006)